*Transactions of the Materials Research Society of Japan* 32[1] 15-18 (2007)

# Structural and Ferroelectric Properties of $Bi_4Ti_3O_{12}/TiO_2$ Thin Films Prepared by Two-Dimensional RF Magnetron Sputtering

Hiroaki Masaya, Naoko Inada, Tohru Higuchi, Takeshi Hattori and Takeyo Tsukamoto
Department of Applied Physics, Tokyo University of Science, 1-3 Kagurazaka, Shinjuku, Tokyo 162-8601, Japan
Fax: 81-3-3260-4772, e-mail: higuchi@rs.kagu.tus.ac.jp

The $Bi_4Ti_3O_{12}$ (BIT) thin films with $TiO_2$ layer were prepared on $Pt/Ti/SiO_2/Si$ substrates by two-dimensional RF magnetron sputtering using $TiO_2$ and $Bi_2O_3$ targets. In order to prevent the interdifussion of BIT thin film, we inserted the $TiO_2$ layer between BIT thin film and Pt electrode. The BIT thin film with $TiO_2$ layer consists of small grain with a diameter of 80 nm. The orientation of BIT thin film depends on the film thickness of $TiO_2$ layer. When the thickness of $TiO_2$ layer is 10 nm, the postannealed BIT thin film exhibited a good *P-E* hysteresis loop. The leakage current ($I_L$) at voltage of 10 V was $10^{-6}$ A/cm$^2$, although the $I_L$ of BIT thin film with no layer was $10^{-5}$ A/cm$^2$.

Key words: $Bi_4Ti_3O_{12}$ (BIT), thin film, two-dimensional RF magnetron sputtering, $TiO_2$ layer, leakage current

## 1. INTRODUCTION

Bismuth layer-structured ferroelectrics $Bi_4Ti_3O_{12}$ (BIT) thin film is expected for application to nonvolatile ferroelectric random access memory (NV-FeRAM) devices with nondestructive readout operation due to its excellent fatigue endurance when in the deposition of this film with Pt electrode [1-3]. In recent years, preparation of BIT thin film has been investigated by several deposition techniques such as sol-gel [4,5], metalorganic decomposition (MOD) [6,7], metalorganic chemical vapor deposition (MOCVD) [8-14], and RF magnetron sputtering [15-21]. From the point of view of commercial production using sol-gel, MOD, and MOCVD methods, there are still some severe difficulties, for instance poor throughput (low deposition rate), high-temperature deposition, compositional nonuniformity across large substrate, rough surface morphology, lack of appropriate precursors in the gas phase, and poor reproducibility. It is well known that the RF magnetron sputtering can prepare high quality thin film with large area. However, detailed techniques of BIT thin film deposition have not been established thus far.

In the present study, the BIT thin films with $TiO_2$ buffer layer have been prepared on the (111)-oriented $Pt/Ti/SiO_2/Si$ substrate by two-dimensional RF magnetron sputtering using $TiO_2$ and $Bi_2O_3$ ceramics targets. The (111)-oriented Pt layer is most commonly inserted as an electrode between the ferroelectric and insulator layers because of its chemical and thermal stability at high temperature. It has been reported that the $TiO_2$ thin film is stable and can prepare using $TiO_2$ target. Therefore, the $TiO_2$ layer might be promising buffer layer, which can avoid the inter diffusion between BIT thin film and Pt substrate. Thus, we discuss in this paper that the $TiO_2$ layer is very effective for prevent of interdifussion.

## 2. EXPERIMENTAL

BIT thin films were deposited by RF magnetron reactive sputtering using $TiO_2$ and $Bi_2O_3$ ceramic multitargets. The $TiO_2$ and $Bi_2O_3$ ceramic targets were prepared as follows [18]. The $TiO_2$ (99.99 %) powder was pressed into disk (5 inch in diameter). The pressed $TiO_2$ disk was sintered at 1250°C for 6 hours. The $Bi_2O_3$ (99.9 %) powder was pressed into disk (5 inch in diameter). The pressed $Bi_2O_3$ disk was sintered at 750°C for 6 hours. The thickness of $Bi_2O_3$ and $TiO_2$ targets was fixed at 4.55 mm and 3.20 mm, respectively. These ceramic targets were examined using XRD analysis.

The deposition system was arranged in a symmetric configuration with a rotating substrate holder for compositional uniformity. The base pressure of the sputtering chamber was typically ~$2\times10^{-8}$ Torr, and substrates were inserted from a load lock into the main chamber to maintain a low base pressure. For the deposition of BIT thin films, an operating pressure of 10 mTorr was maintained during deposition. The total flow rates of Ar and $O_2$ gases were 10 sccm, as controlled by mass-flow controllers, for the stoichiometric thin films. The substrate temperature (Ts) was fixed at about 600°C. The deposition time was usually 60 min. The film thickness was fixed at ~400nm.

The structural properties of the BIT thin films were characterized by XRD. Surface morphology was observed by SEM. Electrical properties were measured using the ferroelectric property measurement system RT-6000HVS. The polarization-electric field (*P-E*) hysteresis loops were measured using one-shot triangular waveforms with a period of 50 ms. The dielectric constant (ε) was measured with LCR meter.

## 3. RESULTS AND DISCUSSION

Figure 1 shows the XRD patterns of $TiO_2$ thin films prepared at $T_s$=400 and 600°C. The $TiO_2$ thin film was prepared using $TiO_2$ ceramic target. The film thickness of $TiO_2$ layer was approximately ~20 nm. A sharp peak Pt (111) a 2θ~40 ° is Pt (111) peak. A weak peak at 2θ=28.5 ° is observed in $TiO_2$ rutile (002) peak.

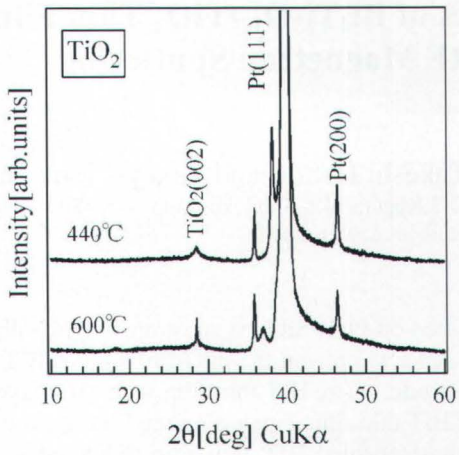


Fig.1: XRD patterns of $TiO_2$ thin films prepared at Ts=400 and 600°C.

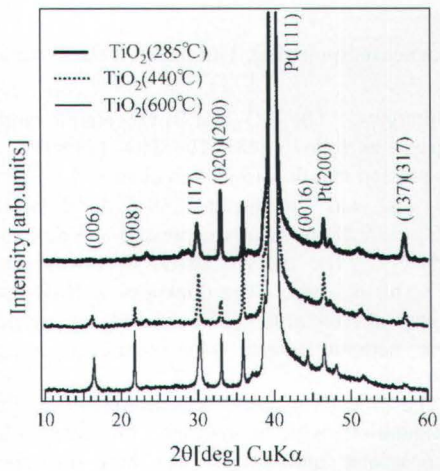


Fig.2: XRD patterns of BIT thin films as a function of Ts of $TiO_2$ thin film.

Comparing each XRD pattern, the c-axis orientation of the thin film is stronger in $T_s$=600°C.

Figure 2 shows the XRD patterns of BIT thin films as a function of Ts of $TiO_2$ thin film. The Ts of BIT thin film was fixed at 600°C. These orientations of XRD patterns are about the same. The prepared BIT thin films exhibit highly *c*-axis orientation, although the (117) peak is also observed in the XRD patterns. This orientation accords with BIT thin film on $TiO_2$ single crystal prepared by MOCVD [22]. The *c*-axis orientation increases with increasing Ts of $TiO_2$ thin film.

Figure 3(a) shows the grain size of BIT thin film as a function of Ts of $TiO_2$ thin film. The grain size of BIT thin film decreases with increasing Ts of $TiO_2$ layer. This result indicates that the crystallization of $TiO_2$ thin film as buffer layer of BIT thin film increases with increasing Ts, as shown in Fig .1, although the reason has been clarified in this study.

Figure 3(b) shows the AFM image of BIT thin film on $TiO_2$ layer prepared at Ts=600°C. As reference, the AFM image of BIT thin film with no buffer layer is also shown in Fig. 3(c). The surface of the BIT thin film is improved by inserting $TiO_2$ layer. The grain size of the BIT thin film with $TiO_2$ layer is smaller than that of the

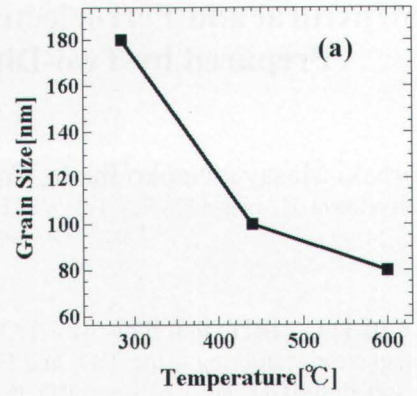


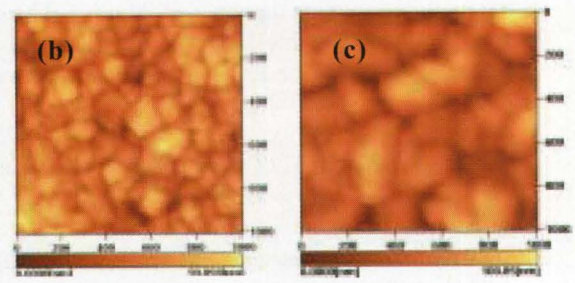


Fig.3: (a) Grain size of BIT thin film as a function of Ts of $TiO_2$ thin film. (b) AFM image of as-deposited BIT thin film on $TiO_2$ thin film prepared at Ts=600°C. (c) AFM image of as-deposited BIT thin film on Pt substrate.

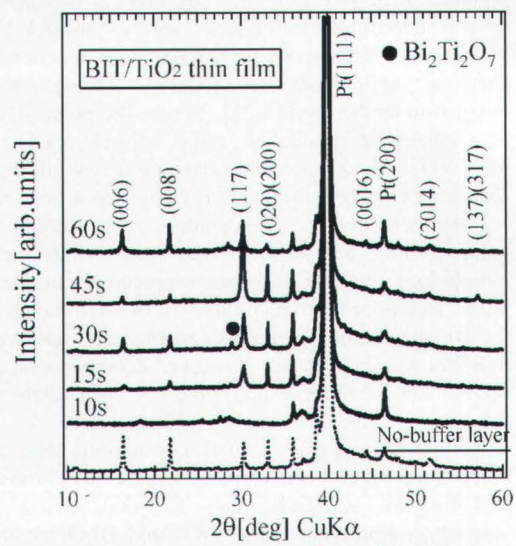


Fig.4: XRD patterns of BIT thin films with $TiO_2$ layer as a function of deposition time of $TiO_2$ layer.

BIT thin film with no buffer layer [23]. The grain sizes of BIT thin films on $TiO_2$ layer and no buffer layer are 80 nm and 200 nm, respectively. The surface roughness ($R_{ms}$) of BIT thin film on $TiO_2$ layer is 90 nm, although that of BIT thin film with no buffer layer is 110 nm. The above results indicate that the BIT thin film with $TiO_2$ layer is high-density thin film.

Figure 4 shows the XRD patterns of BIT thin films with $TiO_2$ layer as a function of deposition time of $TiO_2$ layer. The deposition time is proportional to film thickness of $TiO_2$ layer. When the deposition time of

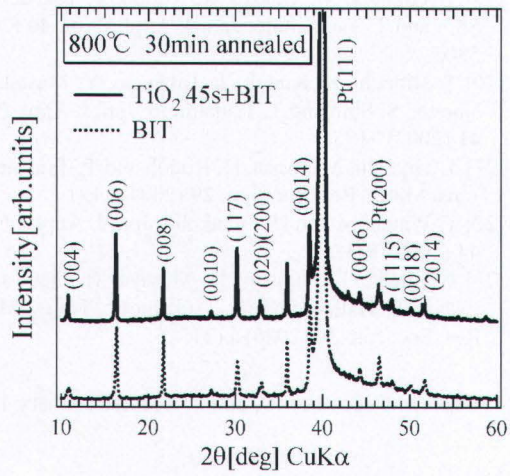


Fig.5: Comparison of XRD patterns between postannealed BIT thin films with $TiO_2$ layer and with no-layer.

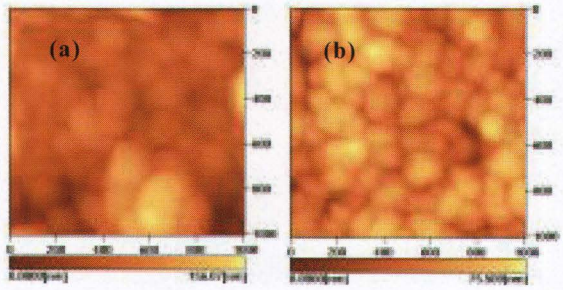


Fig. 6: AFM images of postannealed BIT thin films with (a) no layer and (b) $TiO_2$ layer.

$TiO_2$ layer is below 30 s, the crystallization and orientation of BIT thin film is very low. This contributes to the poor crystallization of $TiO_2$ layer. When the deposition time of $TiO_2$ layer is fixed at above 45 s, the crystallization and orientation of BIT thin film is relatively high. The thickness of $TiO_2$ layer prepared at 45 s is estimated to be 10 nm. In particular, the BIT thin film with $TiO_2$ layer deposited at the deposition time of 45 s exhibits highly (117) orientation. Comparing with BIT thin film with no buffer layer as dashed line, the crystallization and orientation of BIT thin film with $TiO_2$ layer is higher.

Figure 5 shows the XRD patterns of postannealed BIT thin films with $TiO_2$ layer and with no buffer layer. The hysteresis loop of as-deposited BIT thin films were not observed. This originates the oxygen vacancies of BIT thin films. Therefore, these BIT thin films were annealed at 800°C in an $O_2$ atmosphere for 0.5 h in order to investigate the effect of postannealing. The *c*-axis orientations of the BIT thin films increases by postannealing. The orientation is higher in BIT thin film with $TiO_2$ layer.

Figure 6 shows the AFM images of postannealed BIT thin films with $TiO_2$ layer and with no-layer. The grain size of postannealed BIT thin films with $TiO_2$ layer is larger than that of as-deposited BIT thin film on $TiO_2$ thin film as shown in Fig. 3(a). However, the postannealed thin film is improved by inserting $TiO_2$ layer.

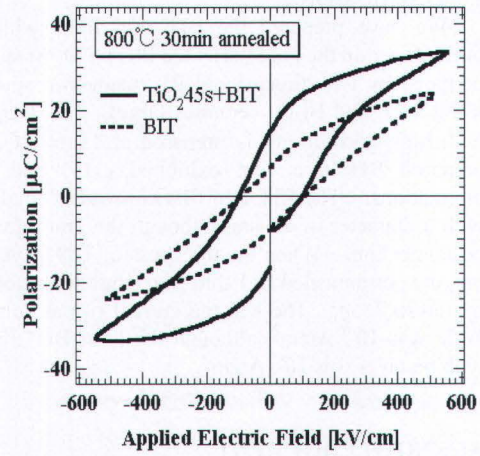


Fig. 7: Hysteresis loops of postannealed BIT thin films with $TiO_2$ layer and with no-layer.

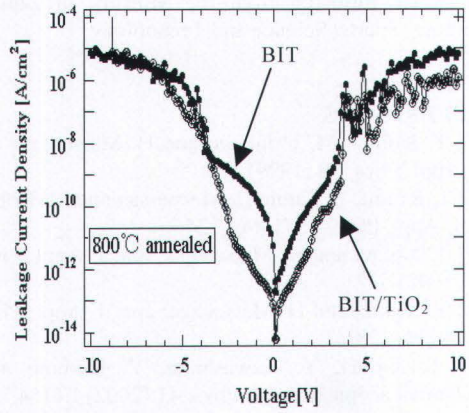


Fig. 8: Leakage current of postannealed BIT thin films with $TiO_2$ layer (open circle) and with no-layer (closed circle).

Figure 7 shows the hysteresis loops of postannealed BIT thin films with $TiO_2$ layer and with no-layer. The hysteresis loops are observed in both thin films. The obtained hysteresis loops exhibit symmetrical shape. Comparing each hysteresis loop, the shape is improved by inserting $TiO_2$ layer. The large remanent polarization of postannealed BIT thin films with $TiO_2$ layer contributes to highly (117) orientation.

Figure 8 shows the leakage currents ($I_L$) of postannealed BIT thin films with $TiO_2$ layer and with no-layer as functions of voltage. In low voltage region below 5 V, the $I_L$ is lower in postannealed BIT thin films with $TiO_2$ layer. At the voltage of 10 V, the $I_L$ of postannealed BIT thin films with $TiO_2$ layer and with no-layer were $10^{-6}$ and $10^{-5}$ A/cm$^2$, respectively.

The improvements of ferroelectric and structural properties for BIT thin film originate that the $TiO_2$ layer acts as buffer layer in order to prevent the interdifussion between Pt substrate and BIT thin film. To further investigate the ferroelectricity of BIT thin films with $TiO_2$ layer, it is necessary to perform more systematic optimizations such as film thickness of $TiO_2$ layer and substrate temperature during the deposition in the future study.

## 4. CONCLUSION

We have prepared the BIT thin films with $TiO_2$ buffer layer on the (111)-oriented Pt/Ti/$SiO_2$/Si substrate prepared by two-dimensional RF magnetron sputtering using $TiO_2$ and $Bi_2O_3$ ceramics targets. The $TiO_2$ layer with high crystallinity is prepared at Ts=600°C. The prepared BIT thin film exhibited (117) and *c*-axis orientations. The BIT thin film consists of small grain with a diameter of 80 nm, although the grain grows by postannealing. When the thickness of $TiO_2$ layer is 10 nm, the postannealed BIT thin film exhibited a good *P-E* hysteresis loop. The leakage current ($I_L$) at voltage of 10 V was $10^{-6}$ A/cm$^2$, although the $I_L$ of BIT thin film with no layer was $10^{-5}$ A/cm$^2$.

## ACKNOWLEDGEMENT

We would like to thank Ms. A. Nishi for her technical support. A Grant-In-Aid supported this work for Scientific Research from the Ministry of Education, Culture, Sports, Science and Technology.

## REFERENCES

[1] T. Kijima, M. Ushikubo and H. Matsunaga: Jpn. J. Appl. Phys. **38** (1999) 127.
[2] T. Kijima, S. Satoh, H. Matsunaga and M. Koba: Jpn. J. Appl. Phys. **35** (1996) 1246.
[3] T. Kijima and H. Matsunaga: Jpn. J. Appl. Phys. **37** (1998) 5171.
[4] T. Kijima and H. Matsunaga: Jpn. J. Appl. Phys. **38** (1999) 2281.
[5] T. Kijima, Y. Kawashima, Y. Idemoto and H. Ishiwara: Jpn. J. Appl. Phys. **41** (2002) L1164.
[6] S. Okamura, Y. Yagi, K. Mori, G. Fujihashi, S. Ando and T. Tsukamoto: Jpn. J. Appl. Phys. **36** (1997) 5889.
[7] M. Yamaguchi and T. Nagatomo: Thin Solid Films **348** (1999) 294.
[8] T. Watanabe and H. Funakubo: Jpn. J. Appl. Phys. **39** (2000) 5211.
[9] T. Watanabe, A. Saiki, K. Saito and H. Funakubo: J. Appl. Phys. **89** (2001) 3934.
[10] T. Watanabe, H. Funakubo, M. Osada, Y. Noguchi and M. Miyayama: Appl. Phys. Lett. **80** (2002) 100.
[11] M. Nakamura, T. Higuchi and T. Tsukamoto: Jpn. J. Appl. Phys. **42** (2003) 5687.
[12] M. Nakamura, T. Higuchi and T. Tsukamoto: Jpn. J. Appl. Phys. **42** (2003) 5969.
[13] M. Nakamura, T. Higuchi Y. Hachisu and T. Tsukamoto: Jpn. J. Appl. Phys. **43** (2004) 1449.
[14] T. Higuchi, M. Nakamura, Y. Hachisu, T. Hattori and T. Tsukamoto: Jpn. J. Appl. Phys. **43** (2004) 6585.
[15] Y. Masuda, H. Masumoto, A. Baba, T. Goto and T. Hirai: Jpn. J. Appl. Phys. **32** (1993) 4043.
[16] W. Jo, S. M. Cho, H. M. Lee, D. C. Kim and J. U. Bu: Jpn. J. Appl. Phys. **38** (1999) 2827.
[17] M. Tanaka, T. Higuchi, K. Kudoh and T. Tsukamoto: Jpn. J. Appl. Phys. **41** (2002) 1536.
[18] K. Kudoh, T. Higuchi, Y. Iwasa, M. Hosomizu and T. Tsukamoto: Proc. Inter. Symp. Appl. Ferro. (ISAF) **XIII** (2002) 167.
[19] T. Higuchi, M. Tanaka, K. Kudoh, T. Takeuchi, S. Shin and T. Tsukamoto: Jpn. J. Appl. Phys. **40** (2001) 5803.
[20] T. Higuchi, K. Kudoh, T. Takeuchi, Y. Masuda, Y. Harada, S. Shin and T. Tsukamoto: Jpn. J. Appl. Phys. **41** (2002) 7195.
[21] T. Higuchi, M. Iwasa, K. Kudoh and T. Tsukamoto: Trans. Mater. Res. Soc. Jpn. **29** (2004) 1121.
[22] T. Watanabe and H. Funakubo: Jpn. J. Appl. Phys. **44** (2005) 1337.
[23] N. Inada, T. Higuchi, H. Masaya, H. Ogawa, M. Iwasa, T. Hattori and T. Tsukamoto: Trans. Mater. Res. Soc. Jpn. **30** (2006) 1121.

(Received December 19, 2006;Accepted January 16, 2007)